Optimal control simulation of the Deutsch-Jozsa algorithm in a two-dimensional double well coupled to an environment

M. Ndong, D. Lauvergnat, X. Chapuisat, and M. Desouter-Lecomte

Citation: J. Chem. Phys. **126**, 244505 (2007); doi: 10.1063/1.2743429
View online: http://dx.doi.org/10.1063/1.2743429
View Table of Contents: http://jcp.aip.org/resource/1/JCPSA6/v126/i24
Published by the American Institute of Physics.

Optimal control simulation of the Deutsch-Jozsa algorithm in a two-dimensional double well coupled to an environment

M. Ndong
Laboratoire de Chimie Physique, Université Paris-Sud, UMR8000, Orsay, F-91405, France and Laboratoire de Chimie Physique, CNRS, UMR0000, Orsay, F-91405, France

D. Lauvergnat
Laboratoire de Chimie Physique, CNRS, UMR000, Orsay F-91405, France and Laboratoire de Chimie Physique, Université Paris-Sud, UMR8000, Orsay F-91405, France

X. Chapuisat
Laboratoire de Chimie Physique, Université Paris-Sud, UMR8000, Orsay F-91405, France and Laboratoire de Chimie Physique, CNRS, UMR0000, Orsay F-91405, France

M. Desouter-Lecomte[a)]
Laboratoire de Chimie Physique, Université Paris-Sud, UMR8000, Orsay F-91405, France; Laboratoire de Chimie Physique, CNRS, UMR0000, Orsay F-91405, France; and Départment de Chimie, Université de Liége, Institut de Chimie B6, Sart-Tilman, B-4000, Liége 1, Belgium

(Received 14 March 2007; accepted 1 May 2007; published online 26 June 2007)

The quantum Deutsch-Jozsa algorithm is implemented by using vibrational modes of a two-dimensional double well. The laser fields realizing the different gates (NOT, CNOT, and HADAMARD) on the two-qubit space are computed by the multitarget optimal control theory. The stability of the performance index is checked by coupling the system to an environment. Firstly, the two-dimensional subspace is coupled to a small number N_b of oscillators in order to simulate intramolecular vibrational energy redistribution. The complete $(2+N_b)$D problem is solved by the coupled harmonic adiabatic channel method which allows including coupled modes up to $N_b=5$. Secondly, the computational subspace is coupled to a continuous bath of oscillators in order to simulate a confined environment expected to be favorable to achieve molecular computing, for instance, molecules confined in matrices or in a fullerene. The spectral density of the bath is approximated by an Ohmic law with a cutoff for some hundreds of cm^{-1}. The time scale of the bath dynamics (of the order of 10 fs) is then smaller than the relaxation time and the controlled dynamics (2 ps) so that Markovian dissipative dynamics is used. © *2007 American Institute of Physics*.
[DOI: 10.1063/1.2743429]

I. INTRODUCTION

Nowadays, the exciting new field of single molecule computing receives growing interest. Classical gates have been implemented on different kinds of logical molecular machines[1–5] making use only of the populations of the states without consideration of the coherences. Logic functions have also been obtained from electronic quantum states of a single molecule.[6,7] On the contrary, quantum computing[8–10] exploits superposed states and entanglement. It has already been implemented with nuclear magnetic resonance,[11–14] optical network,[15] cavity electrodynamics,[16] and ion traps.[17] Quite recently, vibrational or rovibrational molecular states have been suggested to be candidates for information processing using infrared (IR) laser pulses which can operate in a very short time.[18–32] The usual goal of quantum control is designing laser pulses to drive a quantum system towards a specified target state and optimizing the outcome of chemical reactions. In the context of quantum computation, the goal becomes operating unitary transformations. A single universal laser pulse must realize a given unitary transformation on different inputs which are the states of the qubits.[33–35] This type of control is thus more challenging due to the multiple initial states and targets and more demanding about the performance of the control. Quantum computation aims at utilizing parallelism and entanglement.[36] The Deutsch-Jozsa (DJ) algorithm[37,38] is one of the benchmarks. The aim is to identify whether a binary function f acting on the states of N qubits (two-state systems $|0\rangle,|1\rangle$) is constant or balanced, i.e., whether the output is identical for all the inputs 0 or 1 or whether the output is 1 for half the possible inputs and 0 for the other ones. In the simple case of a one-qubit function $f(x)$, the DJ algorithm determines whether it is constant or balanced by a unique evaluation of the function while two queries are necessary in the classical case. It is worthy that quasiclassical computation based on a kinetic description of the evolution of the quantum state populations could also require the same number of function evaluations as in the quantum case.[39] The quantum DJ algorithm has already been experimentally implemented by NMR using different approaches (Ref. 40 and references herein), by using coherent superpositions of Li_2 rovibrational states[41] and in an all-

[a)]Author to whom correspondence should be addressed. Electronic mail: mdesoute@lcp.u-psud.fr

optical device[42] and simulated by using of two IR active modes of acetylene[22] and vibrational states of two electronic states of I_2.[25]

In this work, we simulate the DJ algorithm for a one-qubit binary function by optimal control theory (OCT) by using vibrational states of a two-dimensional (2D) double well. Vibrational states of a double well have already been proposed for realizing quantum gates.[26–28] The aim is to concatenate the laser pulses separately optimized for each of the four steps of the algorithm and analyze the evolution of the vibrational states. The stability of the results is checked versus coupling to an environment and therefore decoherence. Firstly, the 2D subspace is coupled to a small number N_b of oscillators in order to simulate intramolecular vibrational energy redistribution. The complete $(2+N_b)$D problem is solved by the coupled harmonic adiabatic channel method[43–52] (cHAC) which allows considering exactly up to seven degrees of freedom ($N_b=5$). It should also be possible to use alternative approaches, for example, the OCT multiconfiguration time-dependent Hartree method[53] which can take into account a larger number of oscillators[54,55] or the surrogate Hamiltonian method.[56] Secondly, the computational subspace is coupled to a continuous bath of oscillators in order to simulate a confined environment expected to be favorable to achieve molecular computing,[26] for instance, molecules confined in matrices or in a fullerene. The spectral density of the bath is approximated by an Ohmic law with a cutoff for some hundreds of cm^{-1}. The Markovian regime[57,58] is valid when the correlation time of the bath is smaller than the typical time scale over which the system varies appreciably. Previous simulations on the same model have shown that Markovian dynamics is sufficient.[59] The bath correlation time is of the order of 10 fs for a mean frequency of about 400 cm^{-1} at 298 K. They become completely negligible for a mean frequency above 1000 cm^{-1}. These correlation times remain shorter than the duration of each pulse which is of the order of 0.5 ps. Memory effects or non-Markovian dynamics have been discarded in a first approach.

II. VIBRATIONAL QUBITS

The model is represented in Fig. 1. It is a bifurcating region in the ground potential energy surface of the benchmark system $H_3CO \rightarrow H_2COH$. The model is calibrated on an ab initio computation at the QCISD/6-31G** level of quantum theory.[60] Analytical expressions for the potential energy and dipolar momentum surfaces can be found in Refs. 60 and 28, respectively. A deep reactant well is connected to a symmetric double well corresponding to two rotational conformers P and P'. The transfer from the reactant well to the P and P' double well is described by two active coordinates $\mathbf{q}=(\phi,\theta)$, with $\phi \in [-\pi,\pi]$ and $\theta \in [0,\pi]$. These coordinates are the spherical angles of the migrating atom H with respect to the center of the CO bond. The reduced Hamiltonian is given by

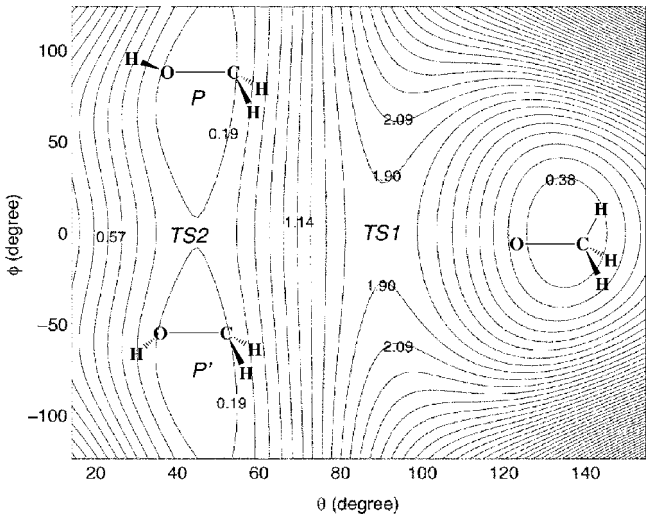

FIG. 1. Isoenergy contours (in eV) in the model potential energy surface of the isomerization $H_3CO \rightarrow H_2COH$ as a function of two active angular coordinates. The zero of energy is at the bottom of the product well (P or P'); the energies of the reactive well and of the transition states, TS1 and TS2, are, respectively, 0.181, 1.854, and 0.195 eV.

$$H_{2D}^{0}(\mathbf{q}) = -\frac{\hbar^2}{2I_\theta}\left(\frac{\partial^2}{\partial\theta^2} + \cot\theta\frac{\partial}{\partial\theta}\right) - \frac{\hbar^2}{2I_\phi}\frac{1}{\sin^2\theta}\frac{\partial^2}{\partial\phi^2} + V(\theta,\phi), \tag{2.1}$$

where Euclidian normalization convention is adopted. The inertia moments are $I_\theta=0.9463\ g\ \text{Å}^2\ \text{mol}^{-1}$ (6160 a.u.) and $I_\phi=0.6805\ g\ \text{Å}^2\ \text{mol}^{-1}$ (4430 a.u.).

The computational basis set contains vibrational states of the P and P' basins. The lower states can be considered as separable and denoted by the quantum numbers of the ϕ and θ oscillators, $|n_\phi n_\theta\rangle = |n_\phi\rangle \otimes |n_\theta\rangle$. The reference qubit $|x\rangle$ on which a one-qubit binary function $f(x)$ acts is formed by the first two vibrational states of the ϕ oscillator $|x\rangle = |0\rangle_\phi$ or $|1\rangle_\phi$. These states are delocalized over the two wells and have even or odd parity. The second qubit is defined by the first two states of the θ oscillator, $|y\rangle = |0\rangle_\phi$ or $|1\rangle_\phi$. The four states of the two qubits $|x\rangle \otimes |y\rangle$ are thus $|\chi_1\rangle = |00\rangle$, $|\chi_2\rangle = |10\rangle$, $|\chi_3\rangle = |01\rangle$, and $|\chi_4\rangle = |11\rangle$. They are represented in Fig. 2.

The molecule is assumed to be aligned in the laboratory axis frame. $\mathbf{e}_z$ is directed along the CO axis. We use two polarization directions $\mathbf{e}_x$ and $\mathbf{e}_y$. The corresponding dipolar functions $\mu_x(\theta,\phi)$ and $\mu_y(\theta,\phi)$ are symmetrical and antisymmetrical functions, respectively.[28] The Hamiltonian in the active subspace reads

$$H_{2D}(\mathbf{q}) = H_{2D}^{0}(\mathbf{q}) - \vec{\mu}\vec{E}(t). \tag{2.2}$$

The surrounding can be taken into account by introducing a model Harmonic Hamiltonian

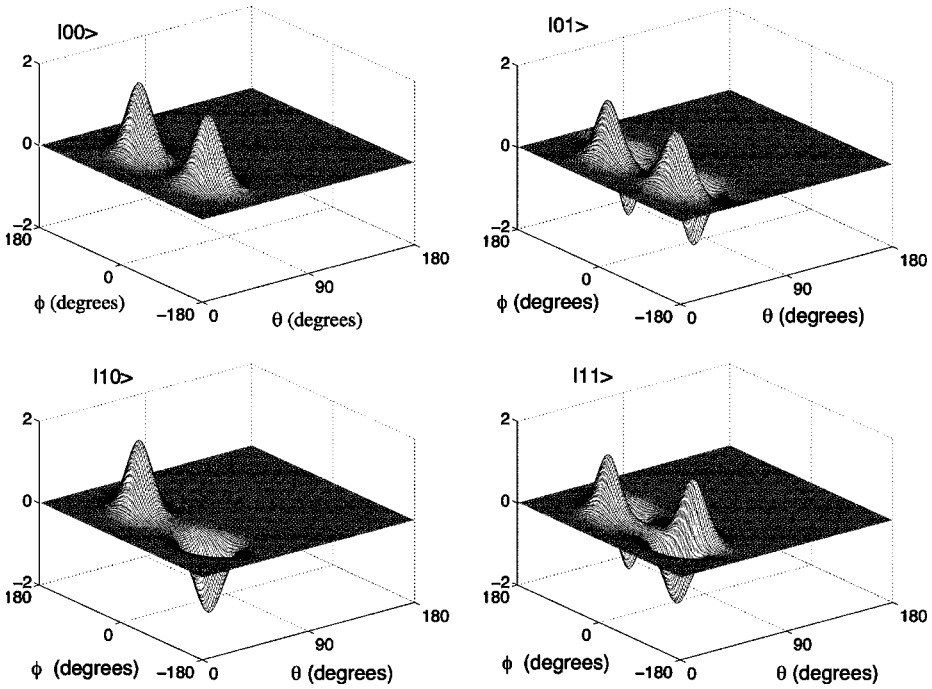

FIG. 2. Vibrational states $|\chi_1\rangle=|00\rangle$, $|\chi_2\rangle=|10\rangle$, $|\chi_3\rangle=|01\rangle$, and $|\chi_4\rangle=|11\rangle$ of the double well potential defining the computational basis set.

$$H^0_{(2+N_b)\mathrm{D}}(\mathbf{Q},\mathbf{q}) = H^0_{2\mathrm{D}}(\mathbf{q}) + H_S(\mathbf{Q};\mathbf{q}) = H^0_{2\mathrm{D}}(\mathbf{q}) + \sum_j^{N_b}\left[\frac{\hat{P}_j^2}{2} + \frac{1}{2}\omega_j^2\left(Q_j - \frac{c_j g(\mathbf{q})}{\omega_j^2}\right)^2\right] \tag{2.3}$$

expressed in mass weighted coordinates. $H_S(\mathbf{Q};\mathbf{q})$ contains a bath Hamiltonian $H_B=\Sigma_j^{N_b}(\hat{P}_j^2+\omega_j^2Q_j^2)/2$, a system-bath coupling linear in the bath coordinates $H_{\mathrm{coupling}}=-g(\mathbf{q})\Sigma_j^{N_b}c_jQ_j$, and a renormalization term $\hat{H}_{\mathrm{renorm}}=\frac{1}{2}g(\mathbf{q})^2\Sigma_{j=1}^{N_b}c_j^2/\omega_j^2$. We choose $g(\mathbf{q})=\cos(\phi)+\sin(\phi)$ adapted to spherical coordinates. This function has an even and an odd part and couples all the eigenvectors according to their parity. The consideration of only the ϕ active coordinate is quite arbitrary. However, the coupling with θ is present indirectly via the anharmonic coupling between θ and ϕ in the potential. The bath spectral density $J(\omega)=(\pi/2)\Sigma_j^{N_b}(c_j^2/\omega_j)\delta(\omega-\omega_j)$ with $J(-\omega)=-J(\omega)$ is approximated by an Ohmic function[57,58]

$$J(\omega) = \lambda^2\frac{\omega}{\omega_c}e^{-|\omega|/\omega_c}, \tag{2.4}$$

where ω_c is the reference frequency corresponding to the maximum of the function. When we consider a finite number of oscillators, the bath spectral density is discretized by

$$c_j^2 = \frac{2}{\pi}\omega_j\frac{J(\omega_j)}{d(\omega_j)}, \tag{2.5}$$

where $d(\omega)$ is the frequency density which is estimated by

$$d(\omega) = \frac{N_b}{\omega_c}\frac{e^{-\omega/\omega_c}}{1-e^{-\omega_m/\omega_c}}, \tag{2.6}$$

with ω_m being the largest frequency of the bath.[54]

TABLE I. One-qubit binary function constant or balanced.

$\|x\rangle$	$f_1(x)$	$f_2(x)$	$f_3(x)$	$f_4(x)$
0	0	1	0	1
1	0	1	1	0

III. ONE-QUBIT DEUTSCH-JOZSA ALGORITHM

The question is to determine whether the binary function $f(x)$ acting on the states of a qubit $|x\rangle$ is constant or balanced. As shown in Table I, two functions f_1 and f_2 are constant by putting two times 0 or 1, respectively, in the $|x\rangle$ qubit. The two functions f_3 and f_4 are balanced by putting alternatively 0 or 1 for f_3 and 1 or 0 for f_4.

The distinction between a constant function (f_1,f_2), and a balanced function (f_3,f_4) requires two queries of the function in a classical process. The DJ algorithm illustrates the use of quantum interferences and thus of superposed states. A single query of the function is then necessary to obtain the global constant or balanced property of the function, in other words, its parity. The trick consists in considering a second qubit $|y\rangle$ and working with superposed states. The four steps of the DJ algorithm are summarized in Fig. 3. The DJ algorithm is usually illustrated and discussed for the initial state $|\chi_1\rangle=|00\rangle$. So we will pay a particular attention to the preparation and transformation of that state. In order to be universal, the gate pulse must be optimized by the multitarget version of OCT (Refs. 19 and 22–24) taking into account all the possible inputs.

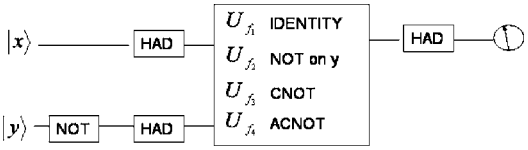

FIG. 3. The four steps of the DJ algorithm for a one-qubit binary function $f(x)$. $|x\rangle$ is the ϕ oscillator and $|y\rangle$ is the θ oscillator.

TABLE II. Inputs and outputs for the four steps of the DJ algorithm.

n	Input	NOT	HADHAD	CNOT	HAD
1	$\|00\rangle$	$\|01\rangle$	$(\|00\rangle-\|01\rangle+\|10\rangle-\|11\rangle)/2$	$(\|00\rangle-\|01\rangle+\|11\rangle-\|10\rangle)/2$	$\|1\rangle_x\otimes(\|0\rangle-\|1\rangle)_y/\sqrt{2}$
2	$\|01\rangle$	$\|00\rangle$	$(\|00\rangle+\|01\rangle+\|10\rangle+\|11\rangle)/2$	$(\|00\rangle+\|01\rangle+\|11\rangle+\|10\rangle)/2$	$\|0\rangle_x\otimes(\|1\rangle+\|0\rangle)_y/\sqrt{2}$
3	$\|10\rangle$	$\|11\rangle$	$(\|00\rangle-\|01\rangle-\|10\rangle+\|11\rangle)/2$	$(\|00\rangle-\|01\rangle-\|11\rangle+\|10\rangle)/2$	$\|0\rangle_x\otimes(\|1\rangle-\|0\rangle)_y/\sqrt{2}$
4	$\|11\rangle$	$\|10\rangle$	$(\|00\rangle+\|01\rangle-\|10\rangle-\|11\rangle)/2$	$(\|00\rangle+\|01\rangle-\|11\rangle-\|10\rangle)/2$	$\|1\rangle_x\otimes(\|0\rangle+\|1\rangle)_y/\sqrt{2}$

Step 1. The NOT gate

$$U_{\mathrm{NOT}}=\begin{pmatrix}0 & 1\\ 1 & 0\end{pmatrix} \tag{3.1}$$

is applied to the $|y\rangle$ qubit. The n possible inputs and their outputs are given in Table II.

Step 2. A HADAMARD gate

$$U_{\mathrm{HAD}}=\left(\frac{1}{\sqrt{2}}\right)\begin{pmatrix}1 & 1\\ 1 & -1\end{pmatrix} \tag{3.2}$$

is applied to each of the $|x\rangle$ and $|y\rangle$ qubits. This double HADAMARD gate is denoted as HADHAD. This step forms a superposed state containing all the states of the two qubits with the same weight. For example, when the input is $|01\rangle$, one gets

$$\begin{aligned}|01\rangle &\rightarrow 1/\sqrt{2}(|0\rangle+|1\rangle)_x\otimes 1/\sqrt{2}(|0\rangle-|1\rangle)_y\\ &=(|00\rangle-|01\rangle+|10\rangle-|11\rangle)/2.\end{aligned} \tag{3.3}$$

All the possibilities are summarized in Table II.

Step 3. The chosen function $f(x)$ (see Table I) is introduced in this step. It is sometimes called "the oracle." In each state of the superposition which is the output of the HADHAD step, the value of x is kept and y is replaced by the sum mod 2 of y and $f(x)$,

$$|x\rangle|y\rangle\rightarrow|x\rangle|y\oplus f(x)\rangle. \tag{3.4}$$

For example, in the case of the function $f_3(x)$ (see Table I) for the particular input $|\chi_1\rangle=|00\rangle$, Eq. (3.4) gives

$$\begin{aligned}|\chi_1^{\mathrm{input,CNOT}}\rangle&=(|00\rangle-|01\rangle+|10\rangle-|11\rangle)/2\rightarrow|\chi_1^{\mathrm{output,CNOT}}\rangle\\ &=(|0(0+0)\rangle-|0(1+0)\rangle+|1(0+1)\rangle\\ &\quad-|1(1+1)\rangle)/2\\ &=(|00\rangle-|01\rangle+|11\rangle-|10\rangle)/2.\end{aligned} \tag{3.5}$$

For each function f, the transformation [Eq. (3.4)] is a unitary transformation corresponding with a well known gate[22] as shown in Fig. 3. U_{f_1} is the identity, and U_{f_2} is the U_{NOT} gate on the $|y\rangle$ qubit (already used in step 1). U_{f_3} is the controlled NOT or CNOT gate which flips the second qubit when the state of the first qubit—or controlled qubit—is 1. U_{f_4} is the ACNOT gate which flips the second qubit when the state of the first qubit is 0. We shall focus on the U_{f_3} example associated with the CNOT gate,

$$U_{\mathrm{CNOT}}=\begin{pmatrix}1 & 0 & 0 & 0\\ 0 & 1 & 0 & 0\\ 0 & 0 & 0 & 1\\ 0 & 0 & 1 & 0\end{pmatrix}. \tag{3.6}$$

All the transformations for the balanced $f_3(x)$ function are summarized in Table II.

Step 4. The $|y\rangle$ qubit is no longer used. A single HADAMARD gate (noted HAD) is applied again to the first qubit $|0,y\rangle\rightarrow(|0,y\rangle+|1,y\rangle)/\sqrt{2}$ and $|1,y\rangle\rightarrow(|0,y\rangle-|1,y\rangle)/\sqrt{2}$. This transformation puts the first qubit $|x\rangle$ in a pure state again which depends on the initial state and on the type of function $f(x)$. For instance, in the particular $n=1$ case, the output of the CNOT step (see Table II) can be rewritten as

$$\begin{aligned}|\chi_1^{\mathrm{output,CNOT}}\rangle=|\chi_1^{\mathrm{input,HAD}}\rangle&=(|00\rangle-|01\rangle+|11\rangle-|10\rangle)/2\\ &=(|0\rangle-|1\rangle)_x\otimes(|0\rangle-|1\rangle)_y/2,\end{aligned} \tag{3.7}$$

so that the HAD gate effectively forms a pure state in $|x\rangle$,

$$|\chi_1^{\mathrm{output,HAD}}\rangle=|1\rangle_x\otimes(|0\rangle-|1\rangle)_y/\sqrt{2}. \tag{3.8}$$

The other cases are gathered in Table II.

In the case where the system is prepared initially in the $|00\rangle$ state, Table III shows that the $|x\rangle$ qubit is finally in the pure state $|0\rangle_x$ if f is constant and in state $|1\rangle_x$ if f is balanced. So a single measure of the $|x\rangle$ qubit state can identify the global property of the function f.

The problem of the relative phase of the target states is important in the context of quantum computation. A strategy to enforce a common phase has been proposed[22] and discussed.[32] This consists in adding a supplementary equation for each gate. In this work, we have not consider this phase problem. In principle, increasing the number of equation ($n_{\max}=2^N+1$) to enforce the phase could be carried out, but we have tried to decrease the computational time, particularly for the adiabatic coupled channel method which is quite time consuming.

TABLE III. Outputs for the last HAD step of the DJ algorithm when the initial state is $\chi_1=|00\rangle$.

$f_k(x)$	Final state
$k=1$	$\|0\rangle_x\otimes(\|0\rangle-\|1\rangle)_y/\sqrt{2}$
$k=2$	$(-\|0\rangle)_x\otimes(\|0\rangle-\|1\rangle)_y/\sqrt{2}$
$k=3$	$\|1\rangle_x\otimes(\|0\rangle-\|1\rangle)_y/\sqrt{2}$
$k=4$	$(-\|1\rangle)_x\otimes(\|0\rangle-\|1\rangle)_y/\sqrt{2}$

IV. DYNAMICAL METHODS

Dynamics is carried out in the Hilbert space when the active subspace is coupled to a finite number of oscillators or in the Liouville space to introduce a coupling to a bath of harmonic oscillators.[57–59,61]

A. Hilbert space

Different monotonically convergent algorithms for solving optimal control problems have been proposed. The objective functional can be defined in different manners[62,63] which are strongly connected.[64] We choose the functional which decouples the boundary conditions for the initial wave packet and the Lagrange multiplier[62] (functional called of type I in a recent analysis[64]). The gate problem is a multitarget case. The functional is then a sum over the different transitions $\chi_n^{\text{output}}=\mathbf{U}_{\text{gate}}\chi_n^{\text{input}}$ corresponding to the gate unitary transformation

$$J=\sum_{n=1}^{2^N}\left\{|\langle\psi_i^n(t_f)|\chi_n^{\text{output}}\rangle|^2-2\,\text{Re}\left[\int_0^{t_f}\langle\psi_i^n(t)|\psi_f^n(t)\rangle\times\langle\psi_f^n(t)|\partial_t+\frac{i}{\hbar}\hat{H}|\psi_i^n(t)\rangle dt\right]\right\}-\alpha\int_0^{t_f}E^2(t)dt, \tag{4.1}$$

where $|\langle\psi_i^n(t_f)|\chi_n^{\text{output}}\rangle|^2$ is the performance index of the nth transformation. $\psi_i^n(t)$ are the wave packets propagated with the optimal field. $E(t)$ and $\psi_f^n(t)$ are the Lagrange multipliers associated with the constraint of satisfying at any time the Schnödinger equation. α is a positive penalty factor which weights the influence of the laser fluence. The procedure to maximize the cost functional under constraint is described in detail in the literature.[65] For an N qubit system, the procedure leads to $(2\times 2^N+1)$ coupled equations.[22] One has to propagate 2^N input wave packets $\psi_i^n(t)$ with an initial condition

$$\psi_i^n(t=0)=\chi_n^{\text{input}},\quad n=1,\ldots,2^N, \tag{4.2}$$

and 2^N output wave packets $\psi_f^n(t)$ with a final condition

$$\psi_f^n(t=t_f)=\chi_n^{\text{output}},\quad n=1,\ldots,2^N. \tag{4.3}$$

The optimal field for a polarization direction along an axis $\mathbf{e}_j$ is given by

$$E_j(t)=-\left(\frac{s(t)}{\hbar\alpha}\right)\text{Im}\sum_{n=1}^{2^N}[\langle\psi_i^n(t)|\psi_f^n(t)\rangle\langle\psi_f^n(t)|\mu_j|\psi_i^n(t)\rangle], \tag{4.4}$$

where $s(t)$ is a switching function $s(t)=\sin^2(\pi t/t_f)$.[65] The equations are solved iteratively.[62] Convergence is improved by using, at each iteration k, $E_j^{(k)}=E_j^{(k-1)}+\Delta E_j^{(k)}$, where $\Delta E_j^{(k)}$ is calculated by Eq. (4.4).[33]

The wave packet formalism is used only when the active 2D subspace is coupled to N_b oscillators $\mathbf{Q}=[Q_1,\ldots,\mathbf{Q}_{N_b}]$ [Eq. (2.3)]. The propagation is carried out by the closed coupled equations in the adiabatic representation.[43–52] The basis set is formed by the products $\varphi_I(\mathbf{q})\xi_U(\mathbf{Q};\mathbf{q})$. $\varphi_I(\mathbf{q})$ are the eigenvectors of the 2D zero order Hamiltonian $H_{2\text{D}}^0(\mathbf{q})$ [Eq. (2.1)] obtained in a primary basis sets of 1600 normalized spherical harmonics ($l_{\max}=39$). The $\xi_U(\mathbf{Q};\mathbf{q})$ basis functions depend parametrically on the active coordinates and are the adiabatic channels. They are the eigenfunctions of the N_b-harmonic Hamiltonian of the surrounding, $H_S(\mathbf{Q};\mathbf{q})=\Sigma_{j=1}^{N_b}[\hat{P}_j^2+\omega_j^2(Q_j-c_jg(\mathbf{q})/\omega_j^2)^2]/2$ [Eq. (2.3)]. Thus, $\xi_U(\mathbf{Q};\mathbf{q})$ are simply the products of N_b 1D-harmonic eigenfunctions and are labeled by means of the excitations in the N_b bath normal modes, j_U. Those retained go from the ground state onwards to some maximal excitations $\max_{\text{excit}}$, or more precisely, $\Sigma_j^{N_b}j_U\leqslant\max_{\text{excit}}$. This method is also named $(2+N_b)$D. After integration over the bath modes, the total Hamiltonian can be rewritten as a matrix in (U,V) of operators acting only on the active variables, $\hat{\mathbf{H}}_{UV}^{\text{eff}}(\mathbf{q},\partial_{\mathbf{q}})$. Since the coupling between the active coordinates and the bath modes is present only in the potential, the general expressions of the effective operators are simplified as follows:

$$\mathbf{H}_{UV}^{\text{eff}}(\mathbf{q},\partial_{\mathbf{q}})=H_{2\text{D}}^0\delta_{UV}+\sum_{i=1}^{N\text{D}}f_{1,UV}^i(\mathbf{q})\partial_i+\Delta V_{UV}^{\text{eff}}(\mathbf{q}), \tag{4.5}$$

where ND is the number of active modes (ND=2 here). The main contribution of the diagonal value of the $\Delta V_{UV}^{\text{eff}}(\mathbf{q})$ matrix is mainly the harmonic energy of the N_b-harmonic oscillators. The diagonal correction, the off-diagonal term of $\Delta V_{UV}^{\text{eff}}(\mathbf{q})$ and $f_{1,UV}^i(\mathbf{q})$ matrices are due to the kinetic contribution associated with the active coordinates of the adiabatic basis functions. In the present study, the initial $|\psi_i^n\rangle$ and target $|\psi_f^n\rangle$ wave packets are

$$|\psi_i^n\rangle=|\chi_n^{\text{input}}\rangle|\xi_0\rangle,\qquad |\psi_f^n\rangle=|\chi_n^{\text{output}}\rangle|\xi_0\rangle, \tag{4.6}$$

where $|\xi_0\rangle$ is the ground basis function of the harmonic bath (U=0).

The propagation of the wave packets has been obtained through the Taylor expansion of the evolution operator[66,67] with an order (here fourth order for a time step of 0.48 fs) which ensures the time reversibility and norm conservation of wave packet. All the integrals are performed numerically with the help of a Gaussian quadrature scheme adapted to the basis set. The integrals and the propagations have been performed with the ELVIBROT program.[51,68] The values of ω_j [Eq. (2.5)] are, respectively, equal to 400 cm^{-1} or 133.3, 266.6, 400, 533.3, and 666.6 cm^{-1} when the number of bath modes N_b used is 1 or 5. Note that the value of the parameter $\max_{\text{excit}}$ is large enough to ensure the convergence of the propagation with the optimal electric field. The variation of the objective of quantum control is around 0.1% when $\max_{\text{excit}}$ increases by 1. In the (2+5)D model, the values of $\max_{\text{excit}}$ is 2 for a parameter λ [Eq. (2.4)] equal to 10^{-3} and the number of harmonic adiabatic channels is 21. In the wave packet formalism, the performance index of a gate is measured by the mean value $O(t_f)=(\Sigma_{n=1}^{2^N}O^n(t_f))/2^N$ of the performance of each transformation given by

$$O^n(t_f)=|\langle\chi_n^{\text{output}}|\psi_i^n(t_f)\rangle|^2. \tag{4.7}$$

B. Liouville space

Several approaches have been proposed to work in the Liouville space.[69–75] We adopt here a monotonically convergent algorithms adapted for the Liouville space.[72] The chosen functional is

$$J = \sum_{n=1}^{2^N} \left\{ |\langle\langle (X_n^{\text{output}})^\dagger | \rho_i^n(t_f)\rangle\rangle|^2 - 2\,\text{Re}\left[\int_0^{t_f} \langle\langle \rho_i^n(t) | \rho_f^n(t)\rangle\rangle \times \left\langle \langle \rho_f^n(t) | \partial_t + \frac{i}{\hbar} L^\dagger | \rho_i^n(t)\rangle \right\rangle dt \right] \right\} - \alpha \int_0^{t_f} E^2(t)dt, \tag{4.8}$$

where L is the total Liouvillian including the interaction with the laser filed and $\langle\langle A|B\rangle\rangle = \text{Tr}(A^\dagger B)$ in the superoperator notation. Optimization leads to propagation of density matrices $\rho_i^n(t)$ with an initial condition X_n^{input} and of $\rho_f^n(t)$ with a final condition X_n^{output}. The density matrices are propagated by the Liouville equation using the Runge-Kutta algorithm,[76]

$$\frac{\partial}{\partial t} \|\rho(t)\rangle\rangle = -\frac{i}{\hbar}\left[L_0 - \sum_j M_j E_j(t) \right] \|\rho(t)\rangle\rangle, \tag{4.9}$$

where $L_0|\rho(t)\rangle\rangle = |\hat{H}_0\rho(t)\rangle\rangle - |\rho(t)\hat{H}_0\rangle\rangle$ and $M_j|\rho(t)\rangle\rangle = |\mu_j\rho(t)\rangle\rangle - |\rho(t)\mu_j\rangle\rangle$. The density matrix is expressed in the basis set of 20 eigenvectors of $H_{2\text{D}}^0(\mathbf{q})$.

The field is then given by

$$E_j(t) = -\left(\frac{s(t)}{\hbar\alpha}\right) \text{Im} \sum_{n=1}^{2^N} [\langle\langle \rho_i^n(t) | \rho_f^n(t)\rangle\rangle \langle\langle \rho_f^n(t) | M_j | \rho_i^n(t)\rangle\rangle], \tag{4.10}$$

and we use the improvement already used for the wave packet formulation.[33] At each iteration, the field is given by $E_j^{(k)} = E_j^{(k-1)} + \Delta E_j^{(k)}$, where $\Delta E_j^{(k)}$ is calculated by [Eq. (4.10)].

In the case of an infinite ensemble of oscillators, the system density matrix is defined by $\rho(t) = \text{Tr}_B\, \sigma_{S\oplus B}(t)$, where Tr_B is the partial trace over the bath degrees of freedom and $\sigma_{S\oplus B}(t)$ is the density matrix of the complete system plus bath space. The reduced evolution equation for $\rho(t)$ is obtained in the framework of the projector formalism of Zwanzig-Nakajima.[57,58,77] We adopt the lowest level of approximation. We neglect initial correlation between the system and bath degrees of freedom, which could be introduced by using a more sophisticated treatment.[78] We do not consider correlation between the laser and the dissipation dynamics.[74,75] Finally, we adopt the Markov approximation which neglects memory effects in the reduced dynamics. Consideration of non-Markovian effects in laser control dynamics can be found in different works.[59,71,73,79] The Markovian regime arises when the correlation time of the bath τ_B is smaller than the typical time scale τ_S over which the system varies appreciably. We choose the Lindblad form because it can be shown that the density matrix of the system ρ remains a positive semidefinite Hermitian operator having $\text{Tr}[\rho] = 1$ and $\text{Tr}[\rho^2] \leqslant 1$.[80,81] Here, the Lindblad equations in the eigenstates of $H_{2\text{D}}^0$ [Eq. (2.1)] take the form

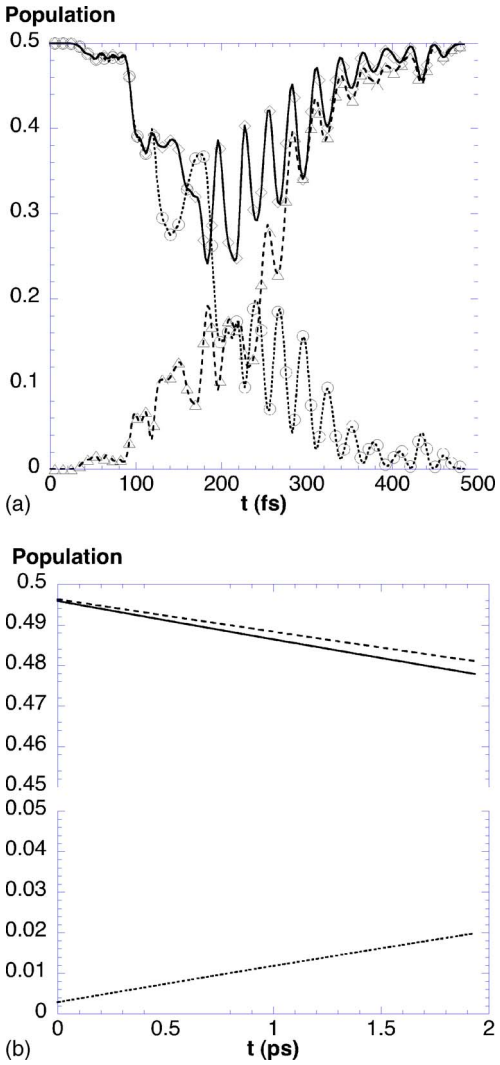

FIG. 4. Population of the first three states, $|00\rangle$ (full line), $|10\rangle$ (dotted line), and $|20\rangle$ (dashed line), (a) during the preparation step with a dissipative dynamics and (b) after the preparation step during a field-free dissipative dynamics. $\lambda = 10^{-3}$ [Eqs. (2.4) and (4.11)].

$$\dot{\rho}_{kl} = -i\frac{\varepsilon_k - \varepsilon_l}{\hbar}\rho_{kl} + \frac{i}{\hbar}\sum_j E_j(t)[\mu_j, \rho(t)]_{kl} + \sum_m -\tfrac{1}{2}[\gamma(\omega_{mk})|A_{mk}|^2 + \gamma(\omega_{ml})|A_{ml}|^2]\rho_{kl},$$

$$\dot{\rho}_{kk} = +\frac{i}{\hbar}\sum_j E_j(t)[\mu_j, \rho(t)]_{kk} + \sum_m [\gamma(\omega_{km})|A_{km}|^2\rho_{mm} - \gamma(\omega_{mk})|A_{mk}|^2\rho_{kk}], \tag{4.11}$$

where $\gamma(\omega) = J(\omega)/(1 - e^{-\beta\omega})$, $\beta = 1/kT$, and $\mathbf{A}$ is the matrix of the function of the active coordinate $g(\mathbf{q})$ [Eq. (2.3)]. In the matrix density formalism, the performance index of a gate is measured by the mean value $O(t_f) = (\Sigma_{n=1}^{2^N} O^n(t_f))/2^N$ of the performance of each transformation given by

$$O^n(t_f) = \langle\langle (X_n^{\text{output}})^\dagger | \rho_i^n(t_f)\rangle\rangle. \tag{4.12}$$

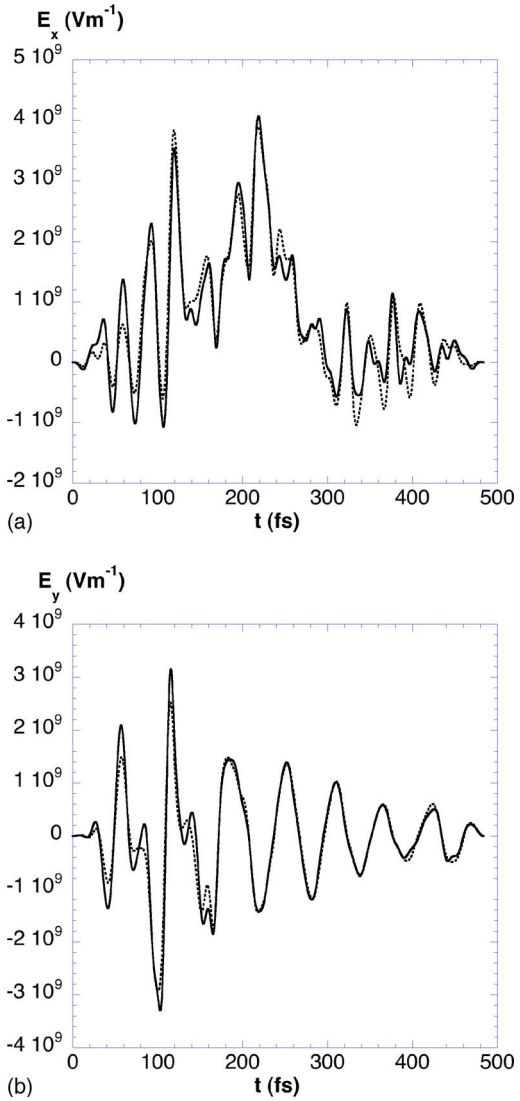

FIG. 5. Two optimal fields for the preparation step obtained with (full line) and without (dotted line) dissipative dynamics: (a) x component and (b) y component. $\lambda = 10^{-3}$ [Eqs. (2.4) and (4.11)].

V. SIMULATION IN THE DOUBLE WELL MODEL

In this section, we first discuss the preparation of the $|00\rangle$ state which is problematic for a double well system where the $|00\rangle$ and $|10\rangle$ states are quasidegenerate. We then study the 2D case by assuming an ideal preparation in a pure state $|00\rangle$. We successively analyze the modifications appearing when the subspace is coupled to a small number of oscillators (cHAC) and to a continuous bath of oscillators (Markovian dynamics). In the last case, we give a complete survey of the evolution of the populations starting from the initial Boltzmann mixture.

A. Preparation of the initial state

As shown in Table II, the pure state in which the $|x\rangle$ qubit is at the end of the process depends on the initial state. For vibrational computers, one has to consider rigorously a Boltzmann ensemble. For high frequency vibrators, one can safely admit that the initial state is $|00\rangle$. However, this is not the case for the double well since the first two levels are

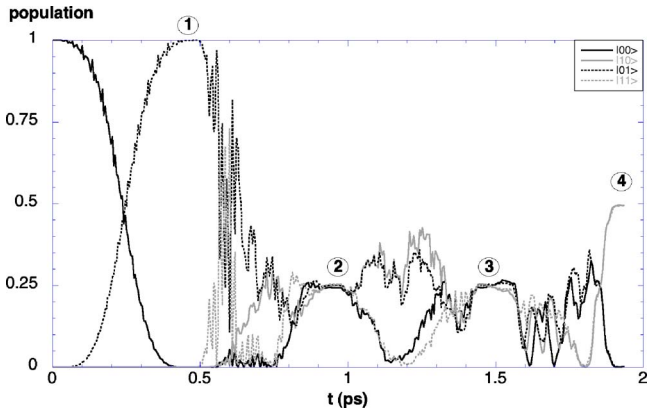

FIG. 6. Population of the four qubit states obtained by propagation with the optimal field for the concatenated four steps of the DJ algorithm (1, NOT on $|y\rangle$; 2, HADHAD on $|x\rangle$ and $|y\rangle$; 3, CNOT, oracle for $f_3(x)$; 4, HAD on $|x\rangle$). The initial state is $|00\rangle$. Black lines: full $|00\rangle$, dashed $|01\rangle$; gray lines: full $|10\rangle$, dashed $|11\rangle$.

quasidegenerate so that they are equally populated. Unfortunately, the $|00\rangle$ state leads to the $|1\rangle_x \otimes (|0\rangle - |1\rangle)_y/\sqrt{2}$ for the $f_3(x)$ function while the state $|10\rangle$ leads to $|0\rangle_x \otimes (|1\rangle - |0\rangle)_y/\sqrt{2}$. An equally weighted mixture of states $|00\rangle$ and $|10\rangle$ will give the results $|1\rangle$ and $|0\rangle$ in the first qubit with the same probability. Inspired by the procedure proposed in order to separate racemic mixture,[82,83] we use an optimal laser pulse to transform the initial mixture and temporarily excite the undesirable $|10\rangle$ state towards the $|20\rangle$ state according to

$$X(t=0) = |00\rangle\tfrac{1}{2}\langle 00| + |10\rangle\tfrac{1}{2}\langle 10|,$$
$$X(t_f) = |00\rangle\tfrac{1}{2}\langle 00| + |20\rangle\tfrac{1}{2}\langle 20|. \tag{5.1}$$

The $|00\rangle$, $|20\rangle$ energy gap is 598 cm^{-1} so that this state is nearly not populated at 300 K (5%). It is worth noting, that this preparation step works well also for other states, such as $|30\rangle$ and $|40\rangle$.

Figure 4(a) shows the evolution of the population of the states $|00\rangle$, $|10\rangle$, and $|20\rangle$ during the preparation step with and without dissipative dynamics. For both dynamics, the residual population in the $|10\rangle$ state is below 3%. As the $|20\rangle$ state is not involved in the algorithm, the situation becomes similar to a pure $|00\rangle$ state. The fields of the preparation step have been optimized without and with dissipation for $\lambda = 10^{-3}$ [Eqs. (2.4) and (4.11)]. They are displayed in Fig. 5. Field-free dissipative dynamics [also shown in Fig. 4(b)] confirms that the $|20\rangle$ state does not relax towards the $|10\rangle$ state during the DJ procedure (2 ps).

B. 2D subspace

Figure 6 shows the population in the four qubit states obtained with the concatenated optimal field when the initial state is assumed to be $\chi_1 = |00\rangle$ and the oracle is the $f_3(x)$ balanced function. Each step of the DJ algorithm has a duration of $t_f = 0.48$ ps and is optimized separately with the ideal input. However, during the propagation with the global optimal field, the computed output of one step is the input for the following one. After the exchange of population of the first NOT (point 1 in Fig. 6), the HADHAD step effectively

TABLE IV. Performance index [Eq. (4.7) and (4.12)] in % for the four steps of the DJ algorithm. The results with the cHAC method are given after 20 iterations (excepted for the HAD step obtained with 100 iterations) and $\alpha=15$, and the values in brackets correspond to the guess field performance.

		2D+Markovian dissipation			
	2D	$\lambda=10^{-3}$	$\lambda=2\times10^{-3}$	(2+1)D $\lambda=10^{-3}$	(2+5)D $\lambda=10^{-3}$
NOT	99.96	99.0	96.5	98.8 (96.6)	98.2 (94.5)
HADHAD	99.61	98.9	96.4	97.4 (92.0)	91.8 (84.2)
CNOT	99.67	98.9	96.4	96.8 (93.7)	90.6 (74.0)
HAD	99.64	99.0	96.3	93.6 (69.9)	89.0 (70.8)

leads to a superposition of the four states with equal weights of 0.25 (point 2 in Fig. 6) as expected from Table II. The CNOT step does not modify the final populations which remain 0.25 (point 3 in Fig. 6). Only the phases of two states are changed. The last HAD step forms the superposition $=(|10\rangle-|11\rangle)/\sqrt{2}$, which corresponds to the pure state $|1\rangle_x$ in the first qubit (point 4 in Fig. 6). Each gate is realized with a performance index larger than 99.5% (see Table IV). The concatenation with the computed outputs decreases a little bit the performance of steps 2–4. One obtains a final performance of 99.05%. This result is slightly larger than the product of all the performances of each step which is 98.88%.

Figure 7 gives the concatenated optimal field. It is well known that a challenge is to design pulses which are experimentally feasible and allow an interpretation of the mechanism. Different attempts to simplify the optimal field have been proposed.[84] One observes that the optimal field notably depends on the zero order field, on the number of polarizations used, and on the value of the α parameter [Eqs. (4.1) and (4.4)]. Here, $\alpha=150$ in each step. The zero order fields for the NOT and the CNOT gates are linearly polarized along $\mathbf{e}_x$. For the NOT, we use the resonance frequency of the transition $|00\rangle\rightarrow|01\rangle$, with an amplitude of 5.142×10^9 V m^{-1}. For the CNOT, two frequencies are used, $|00\rangle\rightarrow|01\rangle$ and $|00\rangle\rightarrow|20\rangle$, with the same amplitude of 2.057×10^9 V m^{-1}. For the two steps containing HADAMARD gates, the trial field is polarized along $\mathbf{e}_x$ and $\mathbf{e}_y$. It is the optimal field previously optimized for the HADAMARD gate on the single $|x\rangle$ qubit.[28,59] This field is robust and allows an interpretation in terms of a Stark effect along the x direction. The optimization over the four transformations distorts it particularly for the double HADAMARD step.

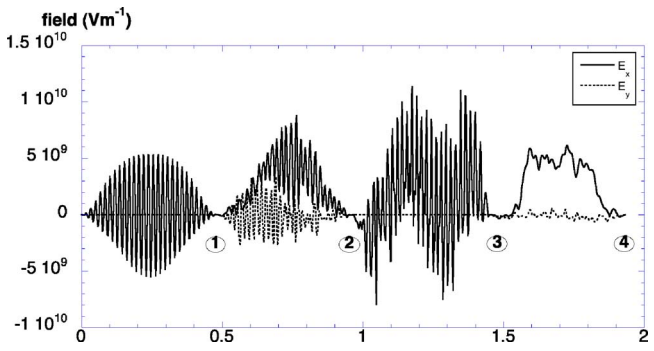

FIG. 7. Optimal field for the four steps of the DJ algorithm (1, NOT on $|y\rangle$; 2, HADHAD on $|x\rangle$ and $|y\rangle$; 3, CNOT, oracle for $f_3(x)$; 4, HAD on $|x\rangle$). Black line: E_x; gray line: E_y.

C. Coupled harmonic adiabatic channels

The system is coupled to one oscillator of frequency 400 cm^{-1} or five oscillators of frequencies 133.3, 266.6, 400, 533.3, and 666.6 cm^{-1} [Eq. (2.3)]. The coefficients c_j [Eq. (2.5)] are chosen to lead to the same coupling strength as in the Markovian case with $\lambda=10^{-3}$. A larger coupling should require too many coupled channels and a too long computational time. The trial field is the OCT field already optimized in the 2D case (see Sec. V B). The results are given after 20 iterations and could be improved but the convergence is very low. General trends can already discussed. The (2+1)D results are satisfactory. This leads to a final performance for the concatenated algorithm of about 90%. Increasing the dimensionality up to (2+5)D decreases the performance. The final population obtained with 20 iterations falls down to about 70% (nearly the product of the values of the separated steps in Table IV). The two delicate steps are the HADAMARD ones.

Figure 8 gives the population of the ground adiabatic channel during the four steps of the DJ algorithm (starting with an ideal initial population). Excited channels are more and more populated particularly during the two HADHAD and HAD steps. The remaining population in the ground

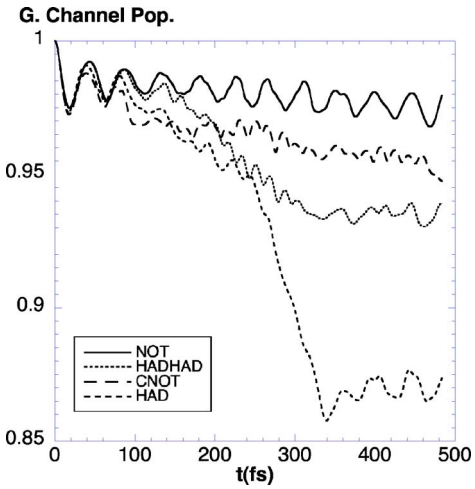

FIG. 8. Population on the ground adiabatic channel during the four steps of the DJ algorithm.

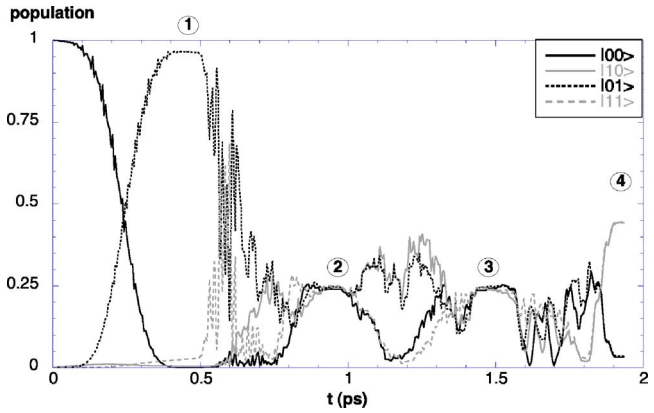

FIG. 9. Population of the four qubit states obtained by Markovian dissipative dynamics ($\lambda=2\times10^{-3}$) with the optimal field of Fig. 7 for the concatenated four steps of the DJ algorithm when the initial state is $|00\rangle$. Black lines: full $|00\rangle$, dashed $|01\rangle$; gray lines: full $|10\rangle$, dashed $|11\rangle$.

channel can be correlated to the performance of the step (see Table IV).

D. Markovian dynamics

We now couple the 2D subspace to an Ohmic bath [Eq. (2.4)] with a reference frequency equal to 400 cm^{-1} a temperature $T=298$ K and different coupling strengths $\lambda=10^{-3}$ and 2×10^{-3}. All the results are gathered in Table IV. In a first approach, we use the optimized field without dissipation as zero order field for the Markovian dynamics. For each step of the DJ algorithm, we have observed that further iterations of the OCT do not improve the results obtained with the optimal field without dissipation. Convergence is reached and no new mechanism is found by the algorithm in order to fight dissipation. So the only effect is a decrease of the performance index due to dissipation during the propagation with the optimal field. The final objective after the concatenation of the four steps falls down to 95% for $\lambda=10^{-3}$ (nearly the product of the values of the separated steps in Table IV) and 86.8% for $\lambda=2\times10^{-3}$. Figure 9 gives the evolution of the populations of the four vibrational states in the case of a large coupling $\lambda=2\times10^{-3}$. The general pattern is not completely destroyed. The two groups of populations (states $|10\rangle$ and $|11\rangle$ on one hand, and $|00\rangle$ and $|01\rangle$ on the other hand) continue to evolve towards a common value but too low for $|10\rangle$ and $|11\rangle$ (0.44) and too large for $|00\rangle$ and $|01\rangle$ (0.03). However, if one admits a tolerance interval of about 10% for the results of the final measure, the DJ remains valid in the presence of this smooth coupling to a bath.

For the steps involving HADAMARD gates, we have also tried to find an optimal field by starting not from the optimal field without dissipation (see Fig. 7) but from the zero order fields used in the one-qubit 2D case.[59] Figure 10 shows the zero order fields of the 2D case and the optimal field obtained for the four-state HAD step without dissipation (already shown in Fig. 7). When this field is taken as zero order for the Markovian dynamics, no further changes are observed so that it is also the optimized field with dissipation. Figure 10 also shows the optimized field obtained with dissipation from the one-qubit 2D zero order field, with the

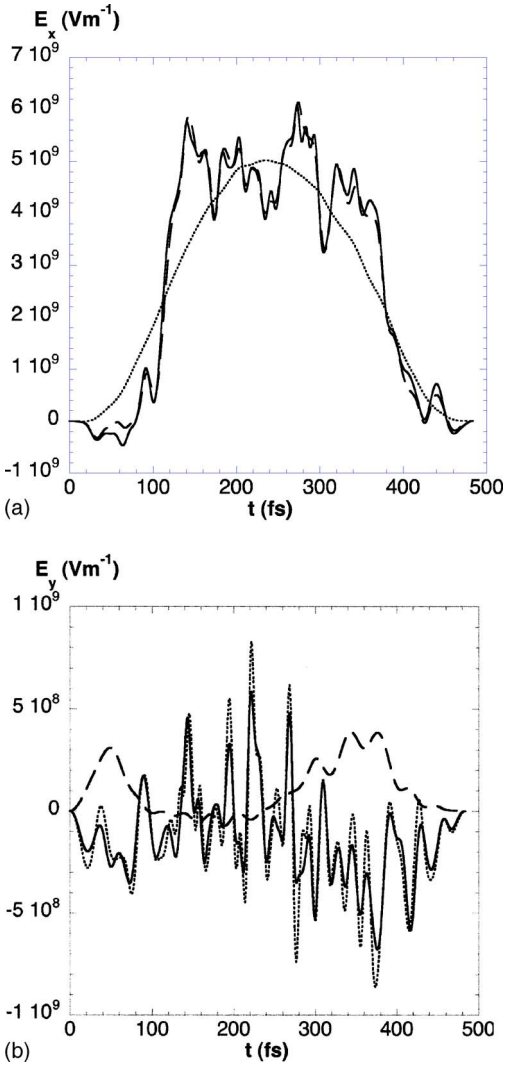

FIG. 10. Two optimal fields for the last HAD step obtained with dissipative dynamics; (a) x component, and (b) y component. The first one (full line) is obtained with the zero order field used to optimize the one-qubit 2D case (Ref. 59) (dashed line). The second one (dotted line) is obtained with the optimized field of the 2D case without dissipation.

same parameter $\alpha=150$ for the HAD step. The fields converge towards the same profile in the two strategies. This confirms that, in this example, the OCT cannot find a different path to avoid dissipation.

Finally, we now give a complete survey of the process including the preparation step starting with a mixture of the $|00\rangle$ and $|10\rangle$ states in the strong dissipative case ($\lambda=2\times10^{-3}$) in order to compare the results with those of the pure state case given in Fig. 9. The field is the universal field computed for the ideal pure state case. For convenience, the origin of the time scale is chosen after the preparation. The upper panel of Fig. 11 shows the increasing population of the transitory state $|20\rangle$ during the preparation. The effect of the universal field is an inversion of population with the $|21\rangle$ state followed by an erratic behavior, which does not interfere with the computational basis set. The lower panel displays the evolution of the qubit states during and after the preparation. The profile is quite similar to that of Fig. 9 starting from the pure ideal state. The asymptotic values of the population of the $|00\rangle$ and $|01\rangle$ states were 0.44 and 0.03,

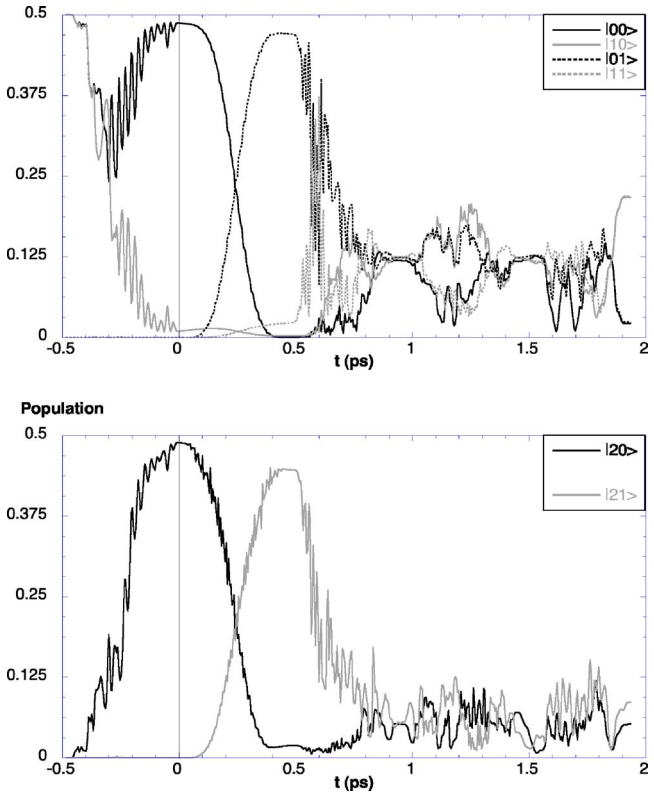

FIG. 11. Population evolution during the whole preparation and DJ algorithm starting with a mixture of the $|00\rangle$ and $|10\rangle$ states with a dissipative dynamics ($\lambda=2\times10^{-3}$) and the universal field optimized for the pure $|00\rangle$ state case.

respectively (in place of 0.5 and 0 in the nondissipative case). They are now 0.22 and 0.02 (in place of 0.25 and 0 in the nondissipative case).

VI. CONCLUDING REMARKS

We have illustrated the realization of the DJ algorithm in a double well potential by concatenation of optimal ultrafast pulses in the IR domain. Two points deserve attention: the preparation of the system in the pure $|00\rangle$ ground state and the effect of decoherence due to the coupling with an environment. The first point arises because the first two $|00\rangle$ and $|10\rangle$ levels are quasidegenerate in a double well. We have shown that OCT could help at exciting the initial population of the $|10\rangle$ towards another state which does not disturb the following evolution of the populations involved in the DJ process. After this preparation step, one practically has a pure $|00\rangle$ state since the higher $|nm\rangle$ states are not populated at room temperature. We have focused on the stability of the results when the active subspace is coupled to some oscillators or to a dissipative bath described by an Ohmic spectral density. In the first case, we recall that cHAC dynamics in a sufficiently large basis set is exact in the framework of the harmonic model. This opens the way to promising simulations up to (2+5)D on more realistic systems by fitting the coupled oscillators on *ab initio* data. For instance, the recent simulation[26] on NH_3 could be treated in full dimensionality in a harmonic model for the inactive oscillators. It would be also possible to go beyond the harmonic approximation if necessary. For more complex systems, the coupling with a bath could be modeled by spectral functions more sophisticated and constructed from an *ab initio* investigation of the inactive modes. In the present example, the optimal control theory in the Markovian dissipation case has not found a new field able to reduce the dissipation. However, some stability has been observed in the evolution of the populations showing that the main features of the algorithm are maintained in the smooth dissipative case. The performance is less satisfactory for the (2+5)D case but for a large coupling. The main difficulty comes from the HADAMARD gates which are typical of the quantum algorithms. However, some quantum computations do mainly use CNOT or TOFFOLI gates which do not involved superposed states.[10,85] It seems that vibrational molecular computing is promising and deserves further exploration.

ACKNOWLEDGMENTS

The computing facilities of IDRIS (Project Nos. 061247 and 2006 0811429) as well as the financial support of the FNRS in the University of Liège SGI Nic project are gratefully acknowledged.

[1] M. M. Mano and C. R. Kime, *Logic and Computer Design Fundamentals* (Prentice-Hall, Upper Saddle River, NJ, 2000).
[2] K. L. Kompa and R. D. Levine, Proc. Natl. Acad. Sci. U.S.A. **98**, 410 (2000).
[3] F. Remacle and R. D. Levine, J. Chem. Phys. **114**, 10239 (2001).
[4] F. Remacle and R. D. Levine, Phys. Rev. A **73**, 033820 (2006).
[5] D. Steinitz, F. Remacle, and R. D. Levine, ChemPhysChem **3**, 43 (2002).
[6] S. Ami, M. Hliwa, and C. Joachim, Chem. Phys. Lett. **367**, 662 (2002).
[7] I. Duchemin and C. Joachim, Chem. Phys. Lett. **406**, 167 (2005).
[8] R. Feynman, Int. J. Theor. Phys. **21**, 467 (1982).
[9] M. A. Nielsen and I. Chuang, *Quantum Computation and Quantum information* (Cambridge University Press, Cambridge, 2000).
[10] G. Benenti, G. Casati, and G. Strini, *Principles of Quantum Computation and Information* (World Scientific, Singapore, 2004).
[11] Z. L. Madi, R. Bruschweiler, and R. R. Ernst, J. Chem. Phys. **109**, 10603 (1998).
[12] T. S. Mahesh, K. Dorai, Arvind, and A. Kumar, J. Magn. Reson. **148**, 95 (2001).
[13] R. Das and A. Kumar, J. Chem. Phys. **121**, 7601 (2004).
[14] M. Mehring, K. Müller, I. S. Averbukh, W. Merkel, and W. P. Schleich, Phys. Rev. Lett. **98**, 120502 (2007).
[15] G. A. Barbosa, Phys. Rev. A **73**, 052321 (2006).
[16] M. Brune, F. Schmidt-Kaler, A. Maali, J. Dreyer, E. Hagley, J. M. Raimond, and S. Haroche, Phys. Rev. Lett. **76**, 1800 (1996).
[17] J. I. Cirac and P. Zoller, Phys. Rev. Lett. **74**, 4091 (1995).
[18] Z. Amitay, R. Kosloff, and S. R. Leone, Chem. Phys. Lett. **359**, 8 (2002).
[19] C. M. Tesch, L. Kurtz, and R. de Vivie–Riedle, Chem. Phys. Lett. **343**, 633 (2001).
[20] C. M. Tesch and R. de Vivie–Riedle, Phys. Rev. Lett. **89**, 157901 (2002).
[21] B. M. R. Korff, U. Troppmann, K. L. Kompa, and R. de Vivie–Riedle, J. Chem. Phys. **123**, 244509 (2005).
[22] C. M. Tesch and R. de Vivie–Riedle, J. Chem. Phys. **121**, 12158 (2004).
[23] U. Troppmann and R. de Vivie–Riedle, J. Chem. Phys. **122**, 154105 (2005).
[24] D. Babikov, J. Chem. Phys. **121**, 7577 (2004).
[25] Y. Ohtsuki, Chem. Phys. Lett. **404**, 126 (2005).
[26] S. Suzuki, K. Mishima, and K. Yamashita, Chem. Phys. Lett. **410**, 358 (2005).
[27] I. R. Sola, V. S. Malinovsky, and J. Santamaria, J. Chem. Phys. **120**, 10955 (2004).
[28] D. Sugny, C. Kontz, M. Ndong, Y. Justum, G. Dive, and M. Desouter-Lecomte, Phys. Rev. A **74**, 043419 (2006).
[29] Y. Teranishi, Y. Ohtsuki, K. Hosaka, H. Chiba, H. Katsuki, and K. Ohmori, J. Chem. Phys. **124**, 114110 (2006).
[30] M. A. Nielsen, M. R. Dowling, M. Gu, and A. C. Doherty, Phys. Rev. A

73 062323 (2006).
[31] T. Cheng and A. Brown, J. Chem. Phys. **124**, 034111 (2006).
[32] M. Zhao and D. Babikov, J. Chem. Phys. **125**, 024105 (2006).
[33] J. P. Palao and R. Kosloff, Phys. Rev. Lett. **89**, 188301 (2002).
[34] J. P. Palao and R. Kosloff, Phys. Rev. A **68**, 062308 (2003).
[35] S. E. Sklarz and D. J. Tannor, Chem. Phys. **322**, 87 (2006).
[36] A. Eckert and R. Jozsa, Proc. R. Soc. London, Ser. A **356**, 1769 (1998).
[37] D. Deutsch, Proc. R. Soc. London, Ser. A **400**, 97 (1985).
[38] D. Deutsch and R. Jozsa, Proc. R. Soc. London, Ser. A **439**, 553 (1992).
[39] F. Remacle and R. D. Levine, Proc. Natl. Acad. Sci. U.S.A. **101**, 12091 (2004).
[40] V. L. Ermakov and B. M. Fung, J. Chem. Phys. **118**, 10376 (2003).
[41] J. Vala, Z. Amitay, B. Zhang, S. R. Leone, and R. Kosloff, Phys. Rev. A **66**, 062316 (2002).
[42] M. S. Tame, R. Prevedel, M. Paternostro, P. Böhi, M. S. Kim, and A. Zeilinger, Phys. Rev. Lett. **98**, 140501 (2007).
[43] W. H. Miller, N. C. Handy, and J. E. Adams, J. Chem. Phys. **72**, 99 (1980).
[44] J. M. Bowman and B. Gazdy, J. Chem. Phys. **93**, 1774 (1990).
[45] J. C. Light and Z. Bacic, J. Chem. Phys. **87**, 4008 (1987).
[46] B. Kuhn, T. R. Rizzo, D. Luckhaus, M. Quack, and M. A. Suhm, J. Chem. Phys. **111**, 2565 (1999).
[47] S. C. Farantos and J. Tennyson, J. Chem. Phys. **84**, 6210 (1986).
[48] B. R. Johnson and W. P. Reinhardt, J. Chem. Phys. **85**, 4538 (1986).
[49] D. Lauvergnat, A. Nauts, Y. Justum, and X. Chapuisat, J. Chem. Phys. **114**, 6592 (2001).
[50] S. Blasco and D. Lauvergnat, Chem. Phys. Lett. **373**, 344 (2003).
[51] D. Lauvergnat and A. Nauts, Chem. Phys. **305**, 105 (2004).
[52] X. Chapuisat and C. Saint-Espès, Chem. Phys. **159**, 391 (1992).
[53] L. Wang, H.-D. Meyer, and V. May, J. Chem. Phys. **125**, 014102 (2006).
[54] H. Wang, J. Chem. Phys. **113**, 9948 (2000).
[55] M. Nest and H.-D. Meyer, J. Chem. Phys. **119**, 24 (2003).
[56] D. Gelman, C. P. Koch, and R. Kosloff, J. Chem. Phys. **121**, 661 (2004).
[57] H.-P. Breuer and F. Petruccione, *The Theory of Open Quantum Systems* (Oxford University Press, Oxford, 2002).
[58] U. Weiss, *Quantum Dissipative Systems* (World Scientific, Singapore, 1999).
[59] D. Sugny, M. Ndong, D. Lauvergnat, Y. Justum, and M. Desouter-Lecomte, J. Photochem. Photobiol., A (in press).
[60] B. Lasorne, G. Dive, D. Lauvergnat, and M. Desouter-Lecomte, J. Chem. Phys. **118**, 5831 (2003).
[61] A. J. Leggett, S. Chakravarty, A. T. Dorsey, M. P. A. Fisher, A. Garg, and W. Zwerger, Rev. Mod. Phys. **59**, 1 (1987).
[62] W. Zhu, J. Bottina, and H. Rabitz, J. Chem. Phys. **108**, 1953 (1998).
[63] W. Zhu and H. Rabitz, J. Chem. Phys. **109**, 385 (1998).
[64] Y. Ohtsuki, G. Turicini, and H. Rabitz, J. Chem. Phys. **120**, 5509 (2004); Y. Ohtsuki, Y. Teranishi, P. Saalfrank, G. Turinici, and H. Rabitz, Phys. Rev. A **75**, 033407 (2007).
[65] K. Sundermann and R. de Vivie–Riedle, J. Chem. Phys. **110**, 1896 (1999).
[66] D. Lauvergnat, S. Blasco, X. Chapuisat, and A. Nauts, J. Chem. Phys. **126**, 204103 (2007).
[67] D. O. Odero, Eur. Phys. J. D **19**, 3 (2002).
[68] D. Lauvergnat, ELVIBROT, quantum dynamics code, 2006, http://www.lcp.u-psud.fr/Pageperso/lauvergnat/perso/
[69] T. Hornung, S. Gordienko, R. de Vivie–Riedle, and B. J. Verhaar, Phys. Rev. A **66**, 043607 (2002).
[70] S. E. Sklarz and D. J. Tannor, Phys. Rev. A **66**, 053619 (2002).
[71] C. Meier and D. J. Tannor, J. Chem. Phys. **111**, 3365 (1999).
[72] Y. Ohtsuki, W. Zhu, and H. Rabitz, J. Chem. Phys. **110**, 9825 (1999).
[73] Y. Ohtsuki, J. Chem. Phys. **119**, 661 (2003).
[74] R. Xu and Y. Yan, J. Chem. Phys. **116**, 9196 (2002).
[75] Y. Mo, R.-X. Xu, P. Cui, and Y. Yan, J. Chem. Phys. **122**, 084115 (2005).
[76] W. H. Press, B. P. Flannery, S. A. Teukolsky, and W. T. Vetterling, *Numerical Recipes* (Cambridge University Press, Cambridge, 1986).
[77] R. Zwanzig, J. Chem. Phys. **33**, 1338 (1960).
[78] I. Burghardt, J. Chem. Phys. **114**, 89 (2001).
[79] M. V. Korolkov, J. Manz, and G. K. Paramonov, J. Chem. Phys. **100**, 10874 (1996).
[80] S. G. Schirmer and A. I. Solomon, Phys. Rev. A **70**, 022107 (2004).
[81] G. Lindblad, Commun. Math. Phys. **48**, 119 (1976).
[82] Y. Ohta, K. Hoki, and Y. Fujimura, J. Chem. Phys. **116**, 7509 (2002).
[83] K. Hoki, L. González, and Y. Fujimura, J. Chem. Phys. **116**, 8799 (2002).
[84] T. Cheng and A. Brown, J. Chem. Phys. **124**, 144109 (2006).
[85] V. Vedral, A. Barenco, and A. Ekert, Phys. Rev. A **54**, 147 (1996).